

Article

# Numerical Investigation of Wind Conditions for Roof-Mounted Wind Turbines: Effects of Wind Direction and Horizontal Aspect Ratio of a High-Rise Cuboid Building

Takaaki Kono <sup>1,\*</sup>, Tetsuya Kogaki <sup>2</sup> and Takahiro Kiwata <sup>1</sup>

<sup>1</sup> Institute of Science and Engineering, Kanazawa University, Kanazawa 920-1192, Japan; kiwata@se.kanazawa-u.ac.jp

<sup>2</sup> National Institute of Advanced Industrial Science and Technology, Koriyama 963-0298, Japan; kogaki.t@aist.go.jp

\* Correspondence: t-kono@se.kanazawa-u.ac.jp; Tel.: +81-76-264-6469

Academic Editor: Frede Blaabjerg

Received: 6 September 2016; Accepted: 25 October 2016; Published: 3 November 2016

**Abstract:** From the viewpoint of installing small wind turbines (SWTs) on rooftops, this study investigated the effects of wind direction and horizontal aspect ratio (HAR = width/length) of a high-rise cuboid building on wind conditions above the roof by conducting large eddy simulations (LESs). The LES results confirmed that as HAR decreases (i.e., as the building width decreases), the variation in wind velocity over the roof tends to decrease. This tendency is more prominent as the angle between the wind direction and the normal vector of the building's leeward face with longer roof edge increases. Moreover, at windward corners of the roof, wind conditions are generally favorable at relatively low heights. In contrast, at the midpoint of the roof's windward edge, wind conditions are generally not favorable at relatively low heights. At leeward representative locations of the roof, the bottoms of the height range of favorable wind conditions are typically higher than those at the windward representative locations, but the favorable wind conditions are much better at the leeward representative locations. When there is no prevailing wind direction, the center of the roof is more favorable for installing SWTs than the corners or the edge midpoints of the roof.

**Keywords:** roof-top; small wind turbine (SWT); wind condition; horizontal aspect ratio; wind direction; large-eddy simulation (LES)

## 1. Introduction

With the increase in the number of small wind turbines (SWTs) installed on the roofs of buildings, there have been reports of some capacity factors being very low [1]. Here, the capacity factor of a wind turbine at a given site is defined as the ratio of the energy actually produced by the turbine to the energy that could have been produced if the machine ran at its rated power over a given time period [2]. Thus, in order to achieve the ideal capacity factors, wind turbines need to be installed in regions where the mean wind speed is sufficiently high. In addition, in order to avoid fatigue failures, wind turbines should ideally be installed in regions where the turbulence intensity is low. There are many published studies on the behavior of wind near buildings (e.g., [3–5]). However, there is limited information regarding wind conditions just above building roofs because most of the studies have focused on the wind load on the buildings, the natural ventilation of the buildings, or on the wind environment near the ground surface.

The existing research on wind conditions for the micro-siting of roof-mounted SWTs can be classified into two types: the first one deals with high-rise buildings [6–8], whereas the second

one deals with low- to mid-rise buildings [9–15]. Blackmore [6] investigated wind conditions by conducting experiments on the roof of a 1:200 scale model building with a full-scale-equivalent length and width of 40 m and 20 m, respectively, and full-scale-equivalent heights of 20, 40, 60, and 80 m. The results showed that the horizontally averaged turbulence intensity tends to converge within 10% of the free-stream turbulence intensity at a height above the roof of 0.12–0.17 times the building height. On the basis of the results, Blackmore [6] recommended setting the heights of horizontal-axis, micro-wind turbines at more than 0.1 times the building height above the roof of a flat-roofed building.

In Kono and Kogaki [7], computational fluid dynamics (CFD) simulations of the flow around a 1:500 scale model building were performed with a full-scale-equivalent length, width, and height of 40, 40, and 80 m, respectively. Many positions where the turbulence intensity exceeded the characteristic values of the normal turbulence model (NTM) of IEC 61400-2 [16] were observed.

With the same building that Kono and Kogaki [7] used, Toja-Silva et al. [8] conducted a CFD analysis of the wind conditions above the roof. Based on European Wind Turbine Standards (Pierik et al. [17]), they recommended placing the rotor of horizontal axis wind turbines (HAWTs) at heights where the turbulence intensity is less than 0.15. In the upstream region above the roof surface, the rotor height should be more than 0.19 times the building height, and in the downstream region, the rotor height should be more than 0.31 times the building height. Below these heights, they recommend using vertical-axis wind turbines (VAWTs), which can be more tolerant of turbulence.

Wind conditions above the roof of a high-rise building can be more favorable for installing SWTs than those of mid- to low-rise buildings. This is because the speed of the approaching wind generally increases with height, and there is less shielding and turbulence from the surrounding buildings [14]. On the other hand, due to the high turbulence intensity near the roof surface, high-rise buildings can require a higher tower and stronger support structure which can be very expensive and can rule out most installations of SWTs [6]. Furthermore, in dense urban areas, it is common for the turbulence intensity at the heights of high-rise buildings to exceed the characteristic value of the NTM of IEC 61400-2 [18]. Therefore, in addition to guidelines for the micro-siting of roof-mounted SWTs, design standards are needed for roof-mounted SWTs that can be set up near the roof surface. To formulate these standards and guidelines, it is important to understand the effects of various factors on the wind conditions above the roof of a high-rise building.

With respect to the CFD turbulence models for this kind of analyses, it is preferable to use large-eddy simulation (LES) type turbulence models, which have higher accuracy for the behavior of the separated flows around buildings than the Reynolds-averaged Navier-Stokes (RANS) turbulence models. For example, Toja-Silva et al. [8] and Mohamed and Wood [19] compared 11 and 6 RANS models, respectively, against the measurements of the flow around the building [20], which Kono and Kogaki [7] also used to validate their LES approach. Most of the RANS models showed significant overestimation of the turbulent kinetic energy or normal stresses upwind of the building. The rest of the RANS models that reproduced the turbulent kinetic energy or normal stresses upwind of the building relatively well showed significant underestimation of the turbulent kinetic energy or normal stresses above the center or downwind of the building. Compared to these RANS simulations, the LES results of Kono and Kogaki [7] showed better agreements in the normal stresses with the measurements [20] upwind, above the center and downwind of the building.

In this study, we investigated the effects of wind direction and the horizontal aspect ratio (HAR = width/length) of a high-rise cuboid building on wind conditions above the roof. This was done by conducting LES of the wind flow around a scale model building with an equivalent height and length of 80 and 40 m, respectively. The respective HARs were 1, 0.5, and 0.25. With five different wind directions, in increments of 22.5°, we discuss the favorable wind conditions for SWT installations and how the favorable turbine locations change as the width of the building decreases. Wind conditions, averaged over 16 wind directions in increments of 22.5°, were also examined for a case where there is no prevailing wind direction.

## 2. Numerical Approach

In this paper, a right-handed Cartesian coordinate system,  $(x_1, x_2, x_3) = (x, y, z)$ , with  $x_3$  being the vertical direction, is used. The velocity components are denoted by  $u_i$  and they include streamwise  $u_1$  ( $=u$ ), lateral  $u_2$  ( $=v$ ), and vertical  $u_3$  ( $=w$ ) components. The numerical simulation code was developed from the open-source computational fluid dynamics (CFD) software FrontFlow/red.

### 2.1. Governing Equations and Discretization Methods

The governing equations for the LES are the filtered continuous equation:

$$\frac{\partial u_i^g}{\partial x_i} = 0 \quad (1)$$

and the filtered Navier-Stokes equations:

$$\frac{\partial u_i^g}{\partial t} + \frac{\partial u_i^g u_j^g}{\partial x_j} = -\frac{1}{\rho} \frac{\partial p^g}{\partial x_i} + 2\nu \frac{\partial S_{ij}}{\partial x_j} - \frac{\partial \tau_{ij}}{\partial x_j} \quad (2)$$

$$S_{ij} = \frac{1}{2} \left\{ \frac{\partial u_i^g}{\partial x_j} + \frac{\partial u_j^g}{\partial x_i} \right\} \quad (3)$$

$$\tau_{ij} = \{u_i u_j\}^g - u_i^g u_j^g \quad (4)$$

where  $u_i$  is the velocity component in the  $x_i$  direction,  $t$  is the time,  $\rho$  is the density of air,  $p$  is the pressure, and  $\nu$  is the kinematic viscosity. The superscript  $g$  denotes filtering at the grid scale. The subgrid-scale (SGS) stresses  $\tau_{ij}$  are computed using the standard Smagorinsky model (S model) [21]:

$$\tau_{ij} = \{C_s f_v \Delta\}^2 \{2S_{ij} S_{ij}\}^{1/2} \quad (5)$$

where  $C_s$  is the Smagorinsky constant,  $\Delta$  is the computational grid scale, and  $f_v$  is Van Driest's damping function [22]:

$$f_v = 1 - \exp\left(-\frac{y^+}{25}\right) \quad (6)$$

$$y^+ = \frac{u_\tau y_n}{\nu} \quad (7)$$

Here,  $u_\tau$  is the friction velocity and  $y_n$  is the distance from the nearest wall. The damping function is used to meet the condition where the value of  $\tau_{ij}$  decreases drastically with a decrease in the distance from the nearest wall and becomes zero on the wall. The optimal value of  $C_s$  varies from flow to flow and even point to point within one flow. To correct the drawback of a constant value of  $C_s$ , several models have been proposed. One of the well-known models is the dynamic Smagorinsky model (DS model) proposed by Germano et al. [23] and revised by Lilly [24], which determines  $C_s^2$  as a variable of space and time following the properties of the flow field, using two filters with different characteristics scales: a grid filter and a test filter. As compared to S model, the accuracy of DS model for the flows around a square cylinder and around a wall-mounted cube is generally improved (e.g., [25–27]). However, DS model has a higher possibility of causing numerical instability [28]. Indeed, our preliminary simulation using DS model diverged, although the cause was not clear. Therefore, we chose to use the S model. The value of  $C_s$  is 0.1, which was used in [25–27].

The governing equations are discretized by the cell vertex finite volume method on a collocated grid system. The advection term is discretized by a combination of 90% of the second-order central difference scheme and 10% of the first-order upwind scheme. Other spatial derivatives are discretized by the central difference scheme. The simplified marker and cell (SMAC) method is used for velocity-pressure coupling. The time integration is performed using the Euler implicit method.

## 2.2. Computational Conditions

The dimensions and HAR of the target building and the wind direction  $\alpha$ , which is defined in Figure 1, are given in Table 1 for all run cases. Here,  $H = 0.16$  m is height of the building. Figure 2 shows the computational domains and grids. The coordinate origin is the center of the building's base. In all run cases, the computational domain extends from  $x = -3.25H$  to  $7.75H$  in the streamwise direction,  $y = -3.438H$  to  $3.438H$  in the span-wise direction, and  $z = 0$  to  $5.625H$  in the vertical direction. In order to examine cases of various wind directions with almost identical computational grids, an O-type grid is used around the building, an unstructured grid is used outside the O-type grid, and a Cartesian grid is used outside the unstructured grid. Except for the rotational angle, the O-type grid is the same among the cases with the same building dimensions and different values of  $\alpha$ . The finest grid sizes around the building surface and over the ground surface are  $0.0025H$  and  $0.0005H$ , respectively. The total numbers of grid points in the cases of HAR = 1.00, 0.50, and 0.25 are  $1.91 \times 10^6$ ,  $2.00 \times 10^6$  and  $2.08 \times 10^6$ , respectively.

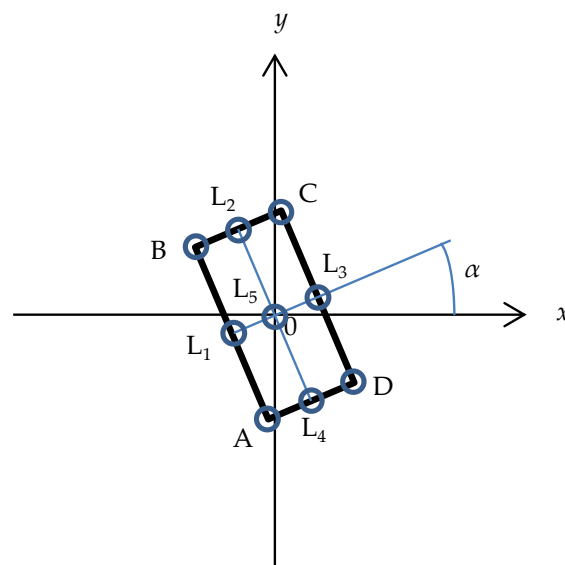


**Figure 1.** Definition of wind direction  $\alpha$  and representative locations on the roof. Circles indicate the representative locations, which are corners A–D, midpoints of an edge  $L_1$ – $L_4$ , and center  $L_5$ .

**Table 1.** List of run cases with various dimensions of the target building and wind directions. Here,  $H = 0.16$  m.

Run Case	Width	Length	Height	HAR	$\alpha$
100_000	$0.5H$	$0.5H$	$H$	1.00	$0^\circ$
100_225	$0.5H$	$0.5H$	$H$	1.00	$22.5^\circ$
100_450	$0.5H$	$0.5H$	$H$	1.00	$45^\circ$
050_000	$0.25H$	$0.5H$	$H$	0.50	$0^\circ$
050_225	$0.25H$	$0.5H$	$H$	0.50	$22.5^\circ$
050_450	$0.25H$	$0.5H$	$H$	0.50	$45^\circ$
050_675	$0.25H$	$0.5H$	$H$	0.50	$67.5^\circ$
050_900	$0.25H$	$0.5H$	$H$	0.50	$90^\circ$
025_000	$0.125H$	$0.5H$	$H$	0.25	$0^\circ$
025_225	$0.125H$	$0.5H$	$H$	0.25	$22.5^\circ$
025_450	$0.125H$	$0.5H$	$H$	0.25	$45^\circ$
025_675	$0.125H$	$0.5H$	$H$	0.25	$67.5^\circ$
025_900	$0.125H$	$0.5H$	$H$	0.25	$90^\circ$

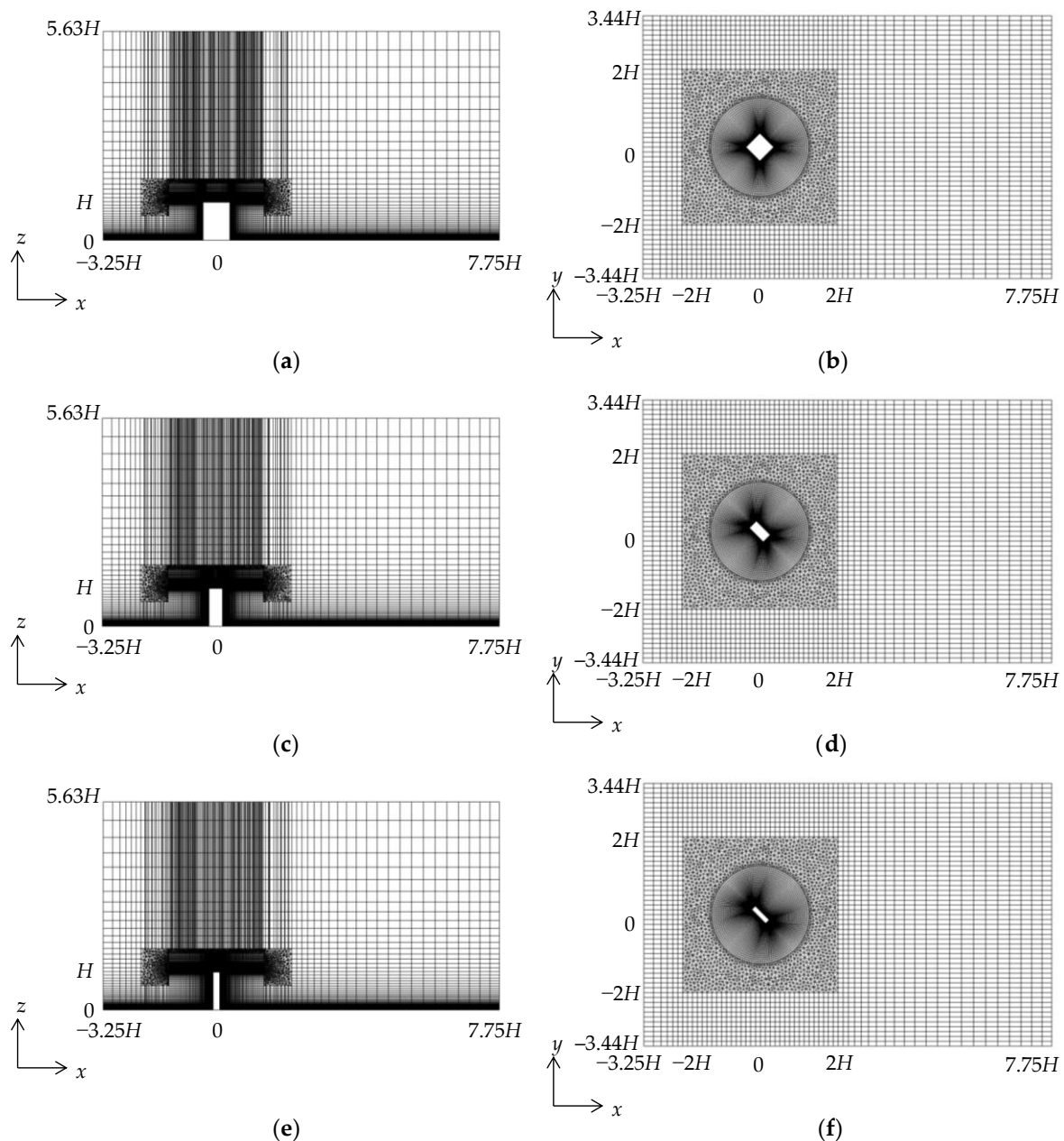


**Figure 2.** Computational domains and grids. (a) Vertical cross section for run case 100\_450 at  $y = 0$ ; (b) Horizontal cross section for run case 100\_450 at  $z = 0$ ; (c) Vertical cross section for run case 050\_450 at  $y = 0$ ; (d) Horizontal cross section for run case 050\_450 at  $z = 0$ ; (e) Vertical cross section for run case 025\_450 at  $y = 0$ ; (f) Horizontal cross section for run case 025\_450 at  $z = 0$ . Here,  $H$  ( $=0.16$  m) is the height of the building.

Table 2 shows the boundary conditions for the velocity and pressure. The time-dependent inflow whose vertical profiles of mean streamwise velocity  $\bar{u}$  and velocity standard deviations  $\sigma_u, \sigma_v, \sigma_w$ , shown in Figure 3, are generated using Kataoka's rescaling approach [29,30] to reproduce the inflow conditions of Meng and Hibi's wind tunnel experiment [20], which assumed the turbulent atmospheric boundary layer over an urban area classified as terrain category IV in the wind loading standards and design criteria of Architectural Institute of Japan [18]. The "law of the wall" conditions for the velocities on the bottom of the computational domain and on the building walls are based on the assumption that the near-wall layer consists (in an instantaneous sense) of a fully viscous sublayer and a fully turbulent superlayer with the interface at  $y^+ = 11$  as follows:

$$\frac{u_p}{u_\tau} = \begin{cases} y^+ & \text{if } y^+ \leq 11, \\ \kappa^{-1} \ln y^+ + 5.5 & \text{otherwise} \end{cases} \quad (8)$$

where  $u_p$  is the instantaneous resolved velocity tangential to the wall at the wall-nearest point, and  $\kappa$  ( $=0.4$ ) is the von Karman constant. In all run cases of this study, the values of  $y^+$  at the wall-nearest points are less than 10. Therefore, it can be considered that the no-slip condition is imposed on the bottom walls of the computational domain and on the building walls.

**Table 2.** Boundary conditions for velocity and pressure.

Boundary	Velocity	Pressure
Inlet ( $x = -3.25H$ )	Time-dependent inflow (Figure 3)	Zero-gradient
Outlet ( $x = 7.75H$ )	Neumann	Zero-gradient
Lateral ( $y = \pm 3.438H$ )	Free-slip	Zero-gradient
Upper ( $z = 5.625H$ )	Free-slip	Zero-gradient
Bottom ( $z = 0$ )	Law of the wall	Zero-gradient
Building wall	Law of the wall	Zero-gradient

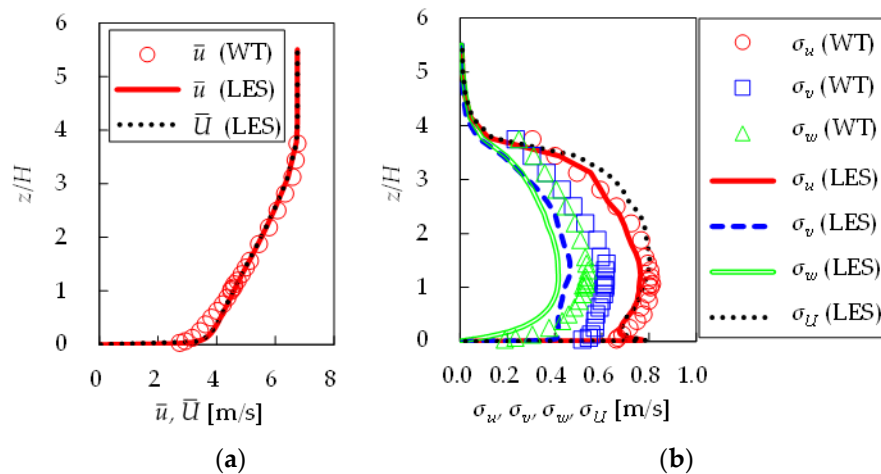


**Figure 3.** Vertical profile of time-dependent inflow. “LES” represents the LES results from the present study, and “WT” represents the wind-tunnel observations from Meng and Hibi [20]. (a) Streamwise mean velocity,  $\bar{u}$ , and horizontal mean velocity,  $\bar{U}$ ; (b) Standard deviations of velocity components in the streamwise direction,  $\sigma_u$ , in the lateral direction,  $\sigma_v$ , in the vertical direction,  $\sigma_w$ , and in the horizontal direction,  $\sigma_U$ .

The values of  $\nu$  and  $\rho$  are  $1.54 \times 10^{-5} \text{ m}^2/\text{s}$  and  $1.184 \text{ kg}/\text{m}^3$ , respectively, both of which are the values for air at  $25 \text{ }^\circ\text{C}$ . The Reynolds number based on the building length ( $0.5H$ ) and  $\bar{u}$  at the building height at the inlet boundary ( $4.23 \text{ m}/\text{s}$ ) is approximately  $2.38 \times 10^4$ . This value is much smaller than the real-world ones. For example, in a case where the wind speed at the height of a full-scale building ( $80 \text{ m}$ ) is  $11 \text{ m}/\text{s}$ , which is equivalent to the rated wind speed of a SWT [31], the Reynolds number based on the building length ( $40 \text{ m}$ ) is  $2.0 \times 10^7$ . It is widely considered that the flow patterns around sharp-edged buildings are dictated by flow separation off the sharp corners and are insensitive to Reynolds number over a wide range of values [32]. Therefore, for building with sharp edge, the necessary relaxation of Reynolds number similarity in wind tunnel tests has little impact on the validity of the results [32]. This concept can also be applied to reduced scale CFD simulations. Therefore, this study assumes that the dependency of the flow characteristics around a rectangular building on Reynolds number is very little and the findings obtained from the reduced scale CFD simulations can be applied to full-scales cases. However, recently, Toja-Silva et al. [33] reported that in their CFD study, there was a significant difference in the vortex structure around roof-mounted solar

panels between a reduced-scale building case and a full-scale building case. As a future study, it is necessary to investigate the effects of Reynolds number on the flow characteristics over the roof of a building using much more computational resources than this study.

The time step is  $2 \times 10^{-4}$  s, and the statistics are summed from 10 to 70 s. The time-average of a flow variable  $\gamma$  is expressed as  $\bar{\gamma}$ . Each simulation was run using 64 cores on a super computing system at Hokkaido University (HITACHI SR16000M1, theoretical peak performance 172 TFLOPS, 176 nodes (5632 cores)) and took approximately 310 h on average.

### 2.3. Validation of Numerical Approach

In Kono and Kogaki [7], we confirmed the validity of the numerical approach by comparing the simulation results for case 100\_000 with the wind tunnel experiment of Meng and Hibi [20]. The simulation results precisely reproduced the mean velocities and velocity standard deviations over the roof and a lateral side of the building at  $0.625H$  from the ground. Figure 4 shows a part of the comparisons, which were presented in Kono and Kogaki [7], of the LES results for case 100\_000 and the wind tunnel measurements of Meng and Hibi [20]. There is a tendency that the LES slightly underestimates the values of  $\sigma_v$  and  $\sigma_w$ . This tendency can be due to the underestimation of  $\sigma_v$  and  $\sigma_w$  by the LES for the inlet boundary conditions shown in Figure 3b. Here, it should be noted that the discrepancies of these normal stresses between the LES results and the wind tunnel measurements in Figure 3b are not significant as compared to the values of  $\sigma_u$  near the roof surface.

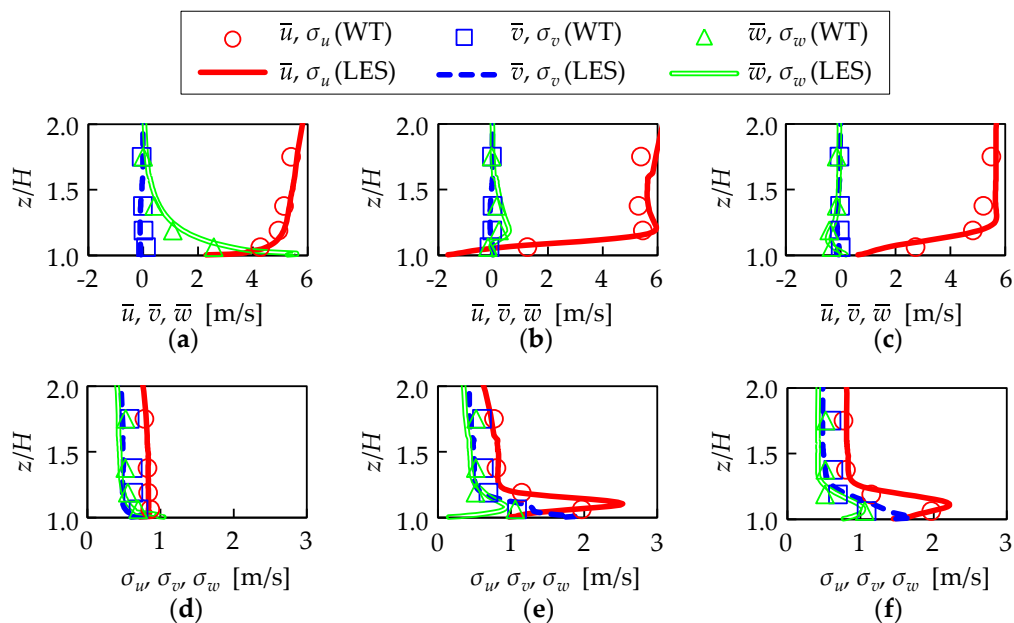


**Figure 4.** Comparisons of the vertical profiles of the mean velocities and velocity standard deviations between the LES results for case 100\_000 and the wind tunnel measurements of Meng and Hibi [19]. “LES” represents the LES results from the present study, and “WT” represents the wind-tunnel observations from Meng and Hibi [20]. (a) Mean velocities at L1; (b) Mean velocities at L5; (c) Mean velocities at L3; (d) Standard deviations at L1; (e) Standard deviations at L5; (f) Standard deviations at L3.

## 3. Results and Discussion

### 3.1. Flow Characteristics over a Roof

Figure 5 shows the LES results of the horizontal distributions of the mean horizontal wind velocity:

$$\bar{U} = \sqrt{\overline{u^2 + v^2}} \quad (9)$$

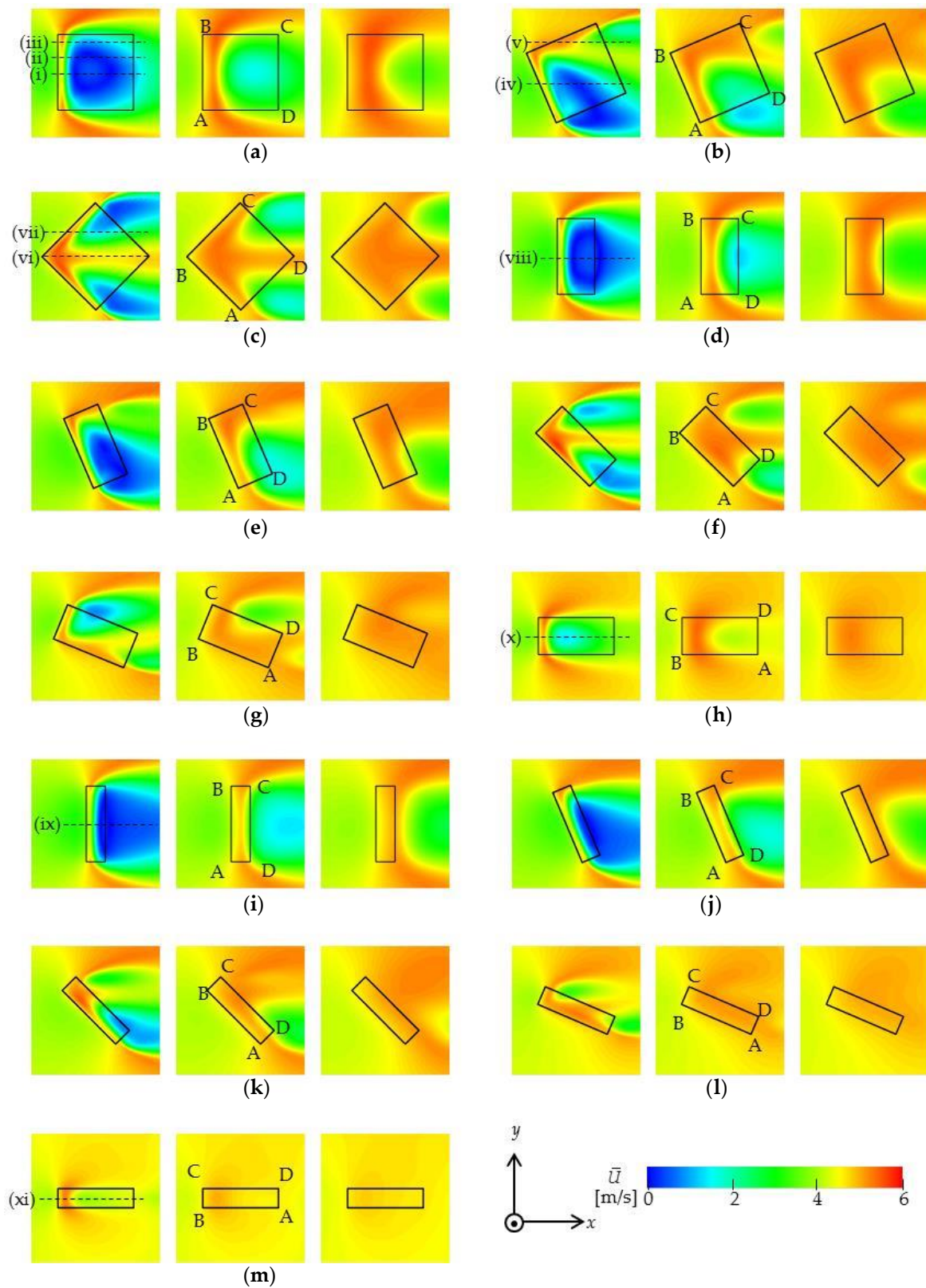


**Figure 5.** Horizontal distributions of the mean horizontal wind velocity at  $z/H = 1.05$  (left), 1.1 (middle) and 1.15 (right). (a) Case 100\_000; (b) Case 100\_225; (c) Case 100\_450; (d) Case 050\_000; (e) Case 050\_225; (f) Case 050\_450; (g) Case 050\_675; (h) Case 050\_900; (i) Case 025\_000; (j) Case 025\_225; (k) Case 025\_450; (l) Case 025\_675; (m) Case 025\_900.

In addition, Figure 6 shows the vertical distributions of the wind vectors along the dotted line indicated in Figure 5. First, the effects of wind direction on the flow pattern over the roof with HAR = 1.0 are examined. In case 100\_000, shown in Figures 5a and 6a–c, the incoming wind flow separates significantly at the overall leading edge AB, and a low-wind-speed region with reverse flow is formed near the roof surface. In case 100\_225, shown in Figures 5b and 6d, it is also seen that the incoming wind flow separates significantly at leading edge AB and that a low-wind-speed region with reverse flow is formed near the roof surface. On the other hand, in Figures 5b and 6e, at leading edge BC, almost no separation occurs, and a high-wind-speed region is formed on the leeward side of the edge. In case 100\_450, shown in Figure 5c, it can be noted that at  $z/H = 1.05$ , there are two low-wind-speed regions due to conical vortices. In Figure 6f, almost no flow separation occurs near corner B, and a high-wind-speed region is formed near the roof surface on its leeward side. On the other hand, as shown in Figure 6g, flow separation occurs at edge BC, and the region of weak wind leeward of the edge is relatively large. From these results, it is understood that wind flow does not always separate significantly at the windward edge of a roof. When the angle between the wind direction and the windward edge of the roof is relatively small ( $22.5^\circ$  or  $45^\circ$ ), flow separation from all or part of the edge is small, and on its leeward side, a region of strong wind tends to form and extends to the vicinity of the roof surface.

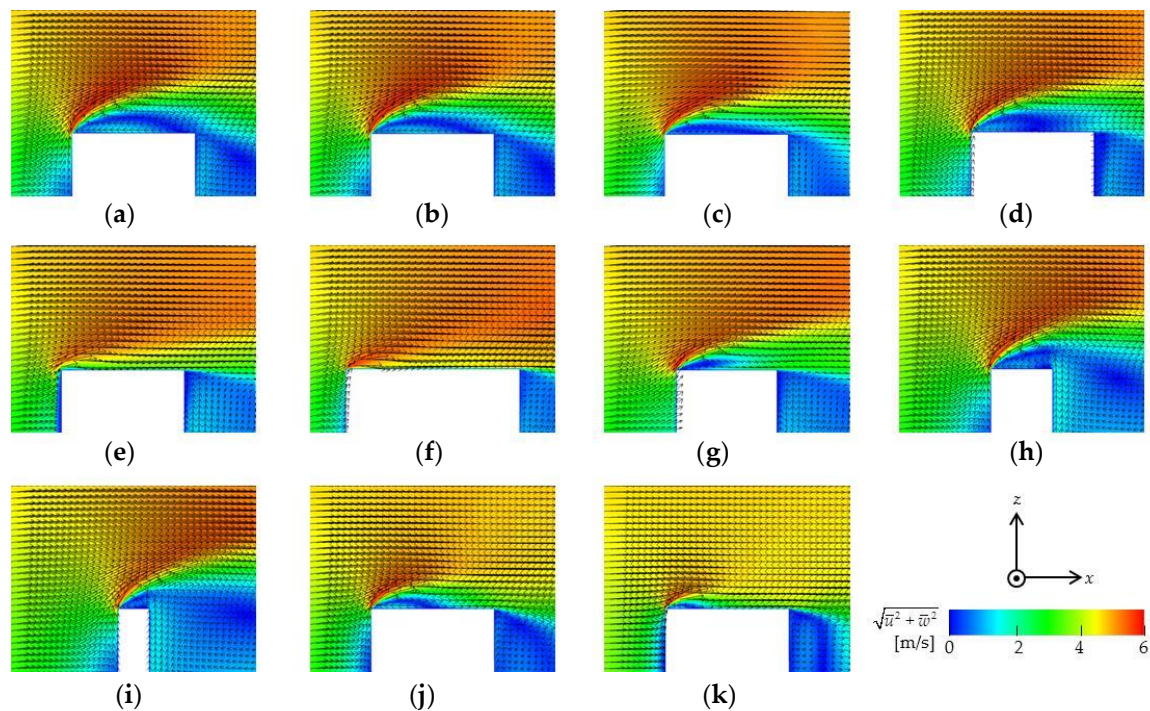


**Figure 6.** Vertical distributions of the wind vectors along the dotted lines indicated in Figure 5. (a) Line i; (b) Line ii; (c) Line iii; (d) Line iv; (e) Line v; (f) Line vi; (g) Line vii; (h) Line viii; (i) Line ix; (j) Line x; (k) Line xi.

Next, the effects of HAR on the flow pattern over the roof are examined. In Figure 5, except for  $\alpha = 90^\circ$ , the flow patterns over the roof with HAR = 0.25 are similar to those over the windward quarter of the roof with HAR = 1.0 (Figure 7a) and similar to those over the windward half of the roof with HAR = 0.5 (Figure 7b). The same is also true, except for  $\alpha = 90^\circ$  for the flow patterns over the roof with HAR = 0.5 and those over the windward half of the roof with HAR = 1.0 (Figure 7c). However, in all cases of  $\alpha$ , there is a tendency for the variation of  $\bar{U}$  over the roof to become smaller with decreasing edge length. This tendency is more prominent as  $\alpha$  increases. When  $\alpha = 0^\circ$ , and the length of the edges parallel to the wind direction decreases, the magnitude of the reverse flow near

the roof surface and that of the augmented velocity near the upper part of the separated shear layer are slightly weakened, as shown in Figure 5a,d,i and Figure 6a,h,i. On the other hand, when  $\alpha = 90^\circ$  and the length of the edges perpendicular to the wind direction decreases, the size of the separation bubble and the variation of  $\bar{U}$  over the roof become significantly smaller (i.e., the magnitude of the augmented velocity near the upper part of the separated shear layer is significantly weakened, and within the leeward area of the separated shear layer or in the area below it, the magnitude of the wind velocity recovers significantly, as shown in Figure 5a,h,m and Figure 6a,j,k). Therefore, it can be said that the development of the height of the separated shear layer in the streamwise direction and the magnitude of the wind velocity over the roof are greatly dependent on the length of the windward edge of the roof.

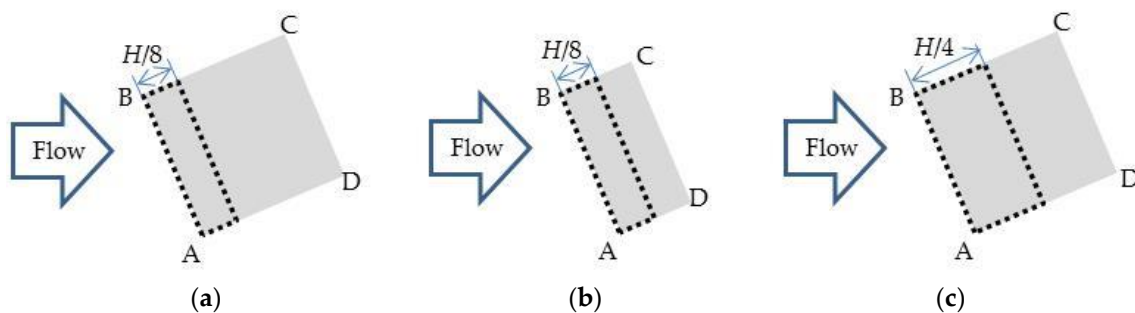


**Figure 7.** Top view of the windward quarter and windward half of the roof. (a) Windward quarter, HAR = 1.00; (b) Windward half, HAR = 0.50; (c) Windward half, HAR = 1.00.

In Figure 8, the horizontal distributions of the standard deviation of  $U$ :

$$\sigma_U = \sqrt{\overline{U^2} - \bar{U}^2} \quad (10)$$

are shown. The definition of  $\sigma_U$  is based on IEC 61400-2 [16]. At every time-step of the LES,  $U$  and  $U^2$  were calculated and used to obtain new values of  $\bar{U}$  and  $\overline{U^2}$ . This procedure is not possible to use for ordinary steady-state RANS simulations. Comparing Figures 5 and 8 for all  $\alpha$  and HAR cases,  $\sigma_U$  is generally low in the regions where  $\bar{U}$  is greater than the streamwise velocity of the same height at the inlet boundary (approximately 4.5 m/s). Such regions can be seen above the vicinity of the leading edges of the roof at  $z/H = 1.05$  and extend to the leeward area at higher heights.

The value of  $\sigma_U$  is also generally low in the regions where  $\bar{U}$  is very low (approximately less than 1.0 m/s). Such regions can be seen in the separated bubbles and conical vortices. There is a tendency for the area of large values of  $\sigma_U$  ( $>1.5$  m/s) at higher heights ( $z/H = 1.1, 1.15$ ) to decrease with an increase in  $\alpha$  or with a decrease in HAR. As with the variation in wind velocity over the roof, this tendency is more prominent as  $\alpha$  increases and HAR decreases.

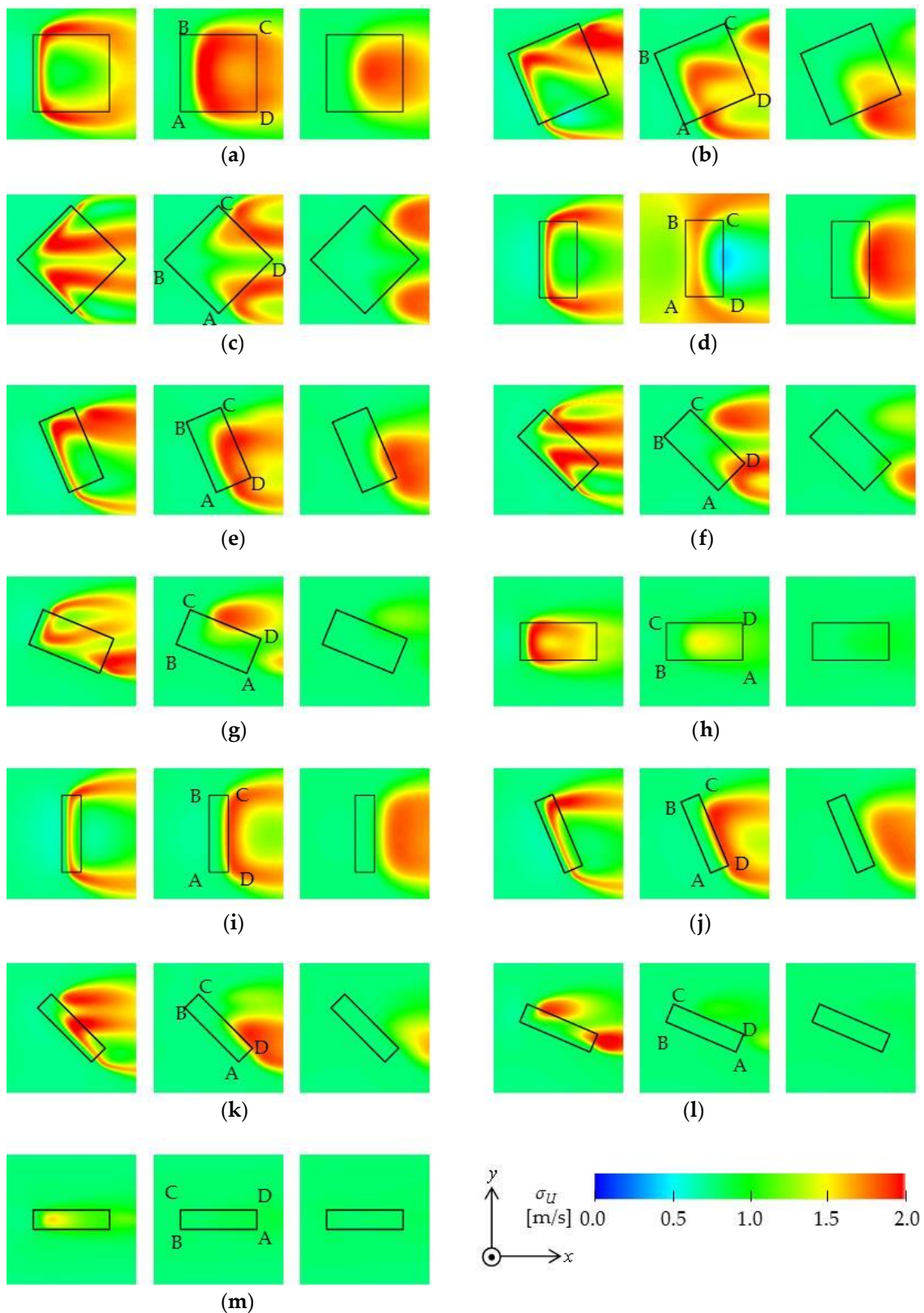


**Figure 8.** Horizontal distributions of the standard deviation of horizontal wind velocity at  $z/H = 1.05$  (left), 1.1 (middle) and 1.15 (right). (a) Case 100\_000; (b) Case 100\_225; (c) Case 100\_450; (d) Case 050\_000; (e) Case 050\_225; (f) Case 050\_450; (g) Case 050\_675; (h) Case 050\_900; (i) Case 025\_000; (j) Case 025\_225; (k) Case 025\_450; (l) Case 025\_675; (m) Case 025\_900.

### 3.2. Wind Conditions at Representative Roof Locations with a Prevailing Wind Direction

In this section, for each wind direction  $\alpha$ , the favorable wind conditions for wind turbine installation and its dependency on HAR are discussed based on Figures 9 and 10. These figures show the vertical profiles of the wind velocity ratio  $\bar{u}/U_0$  and turbulence intensity ratio  $I_U/I_0$ , respectively, at the representative locations on the roof. Here,  $I_U (= \sigma_u/\bar{u})$  is the turbulence intensity;  $U_0$  and  $I_0$  are  $\bar{u}$  and  $I_U$ , respectively, at the inlet boundary (i.e., undisturbed wind) at the same height.

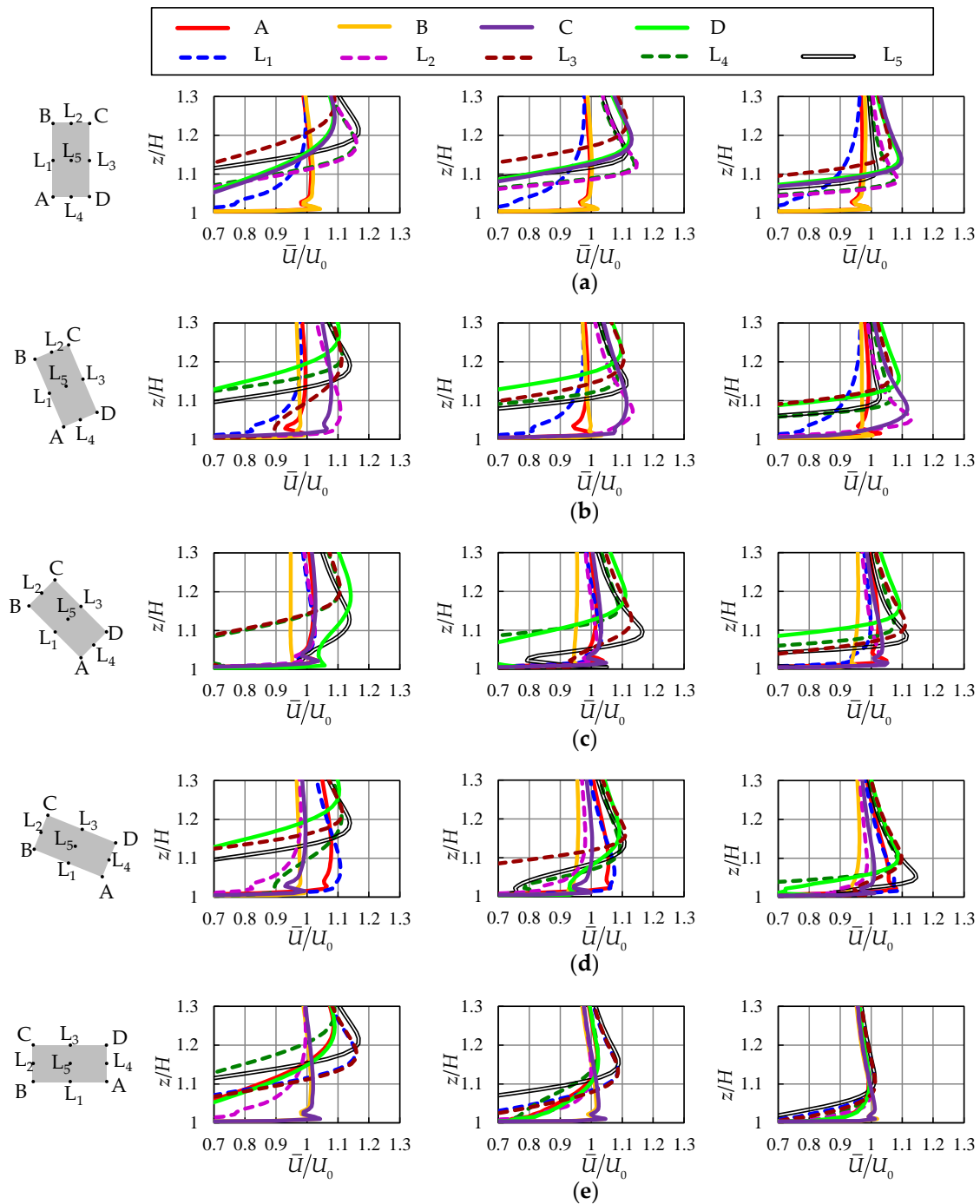


**Figure 9.** Vertical profiles of horizontal wind velocity ratios at the representative locations on the roof: HAR = 1.00 (left), HAR = 0.50 (middle), HAR = 0.25 (right). (a)  $\alpha = 0^\circ$ ; (b)  $\alpha = 22.5^\circ$ ; (c)  $\alpha = 45^\circ$ ; (d)  $\alpha = 67.5^\circ$ ; (e)  $\alpha = 90^\circ$ . In (d,e), the graphs of HAR = 1.00 are obtained by editing the results of cases 100\_225 and 100\_000, respectively, to facilitate the comparison of different HARs.

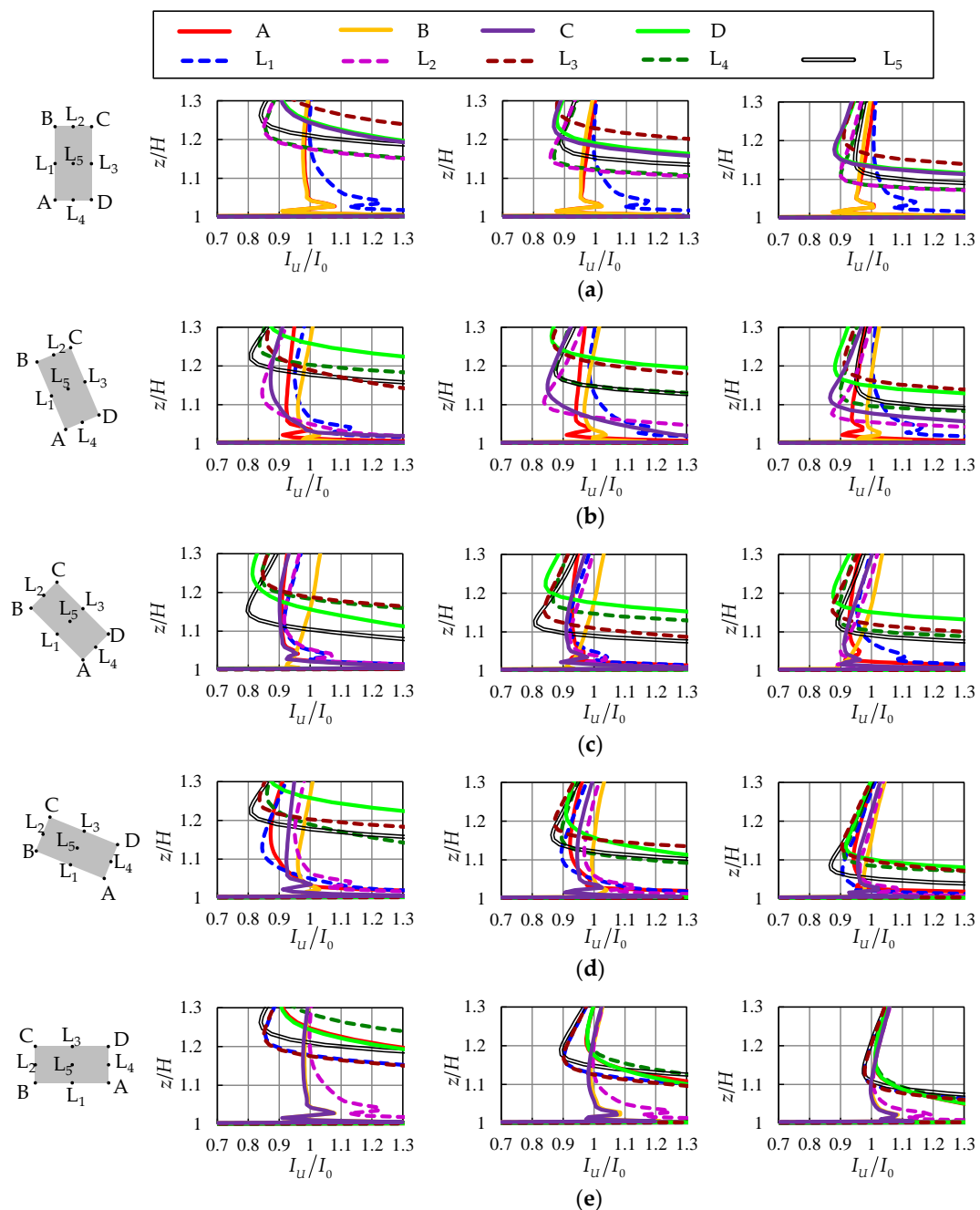


**Figure 10.** Vertical profiles of turbulence intensity ratios at the representative locations on the roof: HAR = 1.00 (left), HAR = 0.50 (middle), HAR = 0.25 (right). (a)  $\alpha = 0^\circ$ ; (b)  $\alpha = 22.5^\circ$ ; (c)  $\alpha = 45^\circ$ ; (d)  $\alpha = 67.5^\circ$ ; (e)  $\alpha = 90^\circ$ . In (d,e), the graphs of HAR = 1.00 are obtained by editing the results of cases 100\_225 and 100\_000, respectively, to facilitate the comparison of different HARs.

The profiles of  $\bar{U}$  and  $\sigma_U$  at the inlet boundary are shown in Figure 3. Since it is common for the turbulence intensity in dense urban areas to exceed the characteristic value of NTM of IEC 61400-2 even at the heights of high-rise buildings [18], we recognize the state of  $I_U/I_0 \leq 1$  as a favorable wind condition for installing SWTs. Regarding a SWT with general wind-durability, it is recommended to install it so that not only the hub but also the whole rotor is within the height range of favorable wind conditions. Table A1 in Appendix A summarizes the height ranges of relatively favorable wind conditions ( $\bar{U}/U_0 \geq 0.97$  and  $I_U/I_0 \leq 1$ ) at the representative locations for all run cases.

### 3.2.1. Wind Direction $\alpha = 0^\circ$

In all of the HAR cases, at windward corners A and B, there is a local peak of  $I_U$  that is due to the motion of the separated shear layer at about  $z/H = 1.03$ . Above the local peak, up to  $z/H = 1.3$ , there is a height range of relatively favorable wind conditions ( $I_U/I_0 \leq 1$  and  $\bar{U}/U_0 \approx 1$ ); the values of  $\bar{U}/U_0$  decrease with a decrease in HAR and are about 0.97 over the height range when HAR = 0.25. The wind power density is proportional to the cube of the wind speed [2]; therefore, at positions where  $\bar{U} = 0.97U_0$ , approximately 90% (or more, if the contribution of  $w$  is considered) of the wind power density of the undisturbed wind of the same height is theoretically available.

Compared to the windward corners, the windward edge's midpoint  $L_1$  is not appropriate for SWT installation at low heights; at  $L_1$ ,  $\bar{U}$  is significantly smaller than  $U_0$ , and  $I_U$  is significantly larger than  $I_0$  in the height range of  $z/H = 1$  to 1.15.

At leeward locations  $L_2$ – $L_5$ , C and D, although the bottoms of the height range where  $I_U/I_0 \leq 1$  are much higher than those at windward corners A and B, the wind conditions in this range are more favorable because the values of  $I_U$  and  $\bar{U}$  are significantly smaller and larger, respectively, than those at the windward corners. With a decrease in HAR, the bottoms of the height range of favorable wind conditions at the leeward locations become lower because the distance from the leading edge becomes shorter resulting in a lower height of the separated shear layer, and also because a variation of  $\bar{U}$  and the values of  $\sigma_U$  become slightly smaller, as discussed in Section 3.1. The order of the bottoms of the height range at the leeward locations does not change with a decrease in HAR. At  $L_2$  and  $L_4$ , the bottoms of the height range are the lowest among the leeward locations.

### 3.2.2. Wind Direction $\alpha = 22.5^\circ$

At windward corners A and B, for all HAR cases, there is a local peak of  $I_U$  at about  $z/H = 1.02$ – $1.03$ . While the maximum value of the local peak exceeds  $I_0$  at corner B in all HAR cases, the maximum value of the local peak at corner A decreases as HAR decreases and is less than  $I_0$  when HAR = 0.5 and 0.25. From about the height of the local peak of  $I_U$  to  $z/H \approx 1.2$  (or even higher) at windward corners A and B, for all HAR cases, there is a height range of relatively favorable wind conditions ( $\bar{U}/U_0 > 0.97$  and  $I_U/I_0 \leq 1$ ).

At windward corner C, the wind conditions where  $I_U/I_0 \leq 1$  are generally much better than those at corners A and B, since  $\bar{U}$  and  $I_U$  are significantly larger and smaller, respectively. The bottom of the height range of favorable wind conditions ( $\bar{U}/U_0 \geq 1$  and  $I_U/I_0 \leq 1$ ) is low ( $z/H \approx 1.03$ ) when HAR = 1.0 and increases with a decrease in HAR, and when HAR = 0.25, the bottom of the height range is relatively high ( $z/H \approx 1.08$ ). Among all windward corners in all  $\alpha$  and HAR cases, the tendency of the bottom of the height range becoming significantly higher with a decrease in HAR is recognized only at corner C when  $\alpha = 22.5^\circ$ .

Similar to corner C, at the windward-edge's midpoint  $L_2$ , the wind conditions where  $I_U/I_0 \leq 1$  and  $\bar{U}/U_0 > 1$  are favorable. However, the dependency of the bottom of the height range of favorable wind conditions on HAR at  $L_2$  is much smaller as compared to that at corner C.

With regard to the windward-edge's midpoint  $L_1$ , the wind conditions are not favorable at low heights ( $z/H \leq 1.1$ ) as compared to those at other windward locations because  $\bar{U}/U_0$  is significantly smaller in all HAR cases and also because  $I_U/I_0 > 1$  in cases of HAR = 0.5 and 0.25.

At leeward locations  $L_3$ – $L_5$  and D, the bottoms of the height range of favorable wind conditions ( $\bar{U}/U_0 \geq 1$  and  $I_U/I_0 \leq 1$ ) are generally higher than those at the windward locations except at  $L_1$ . However, the favorable wind conditions at these locations are apparently better than those at the windward locations except at C and  $L_2$ . With a decrease in HAR, the bottom of the height range at the leeward locations becomes lower except at  $L_3$ . At this location, the bottom of the height range, where  $I_U/I_0 \leq 1$ , is higher when HAR = 0.5 than when HAR = 1.0. This tendency is different from that of  $\alpha = 0^\circ$ , in which with a decrease in HAR, the bottom of the height range at all leeward locations becomes lower. With a change in HAR, the leeward location where the bottom of the favorable wind conditions is the lowest also changes. This tendency is also different from that of  $\alpha = 0^\circ$ .

### 3.2.3. Wind Direction $\alpha = 45^\circ$

In all HAR cases, at windward corners A and C, there is a height range of favorable or relatively favorable wind conditions where  $I_U/I_0 \leq 1$  and  $\bar{U}/U_0 \geq 1$  or at least  $\bar{U}/U_0 \geq 0.97$  from low heights ( $z/H \approx 1.01$ – $1.02$ ) to higher heights ( $z/H \approx 1.3$  or higher).

At the windward-edge's midpoints  $L_1$  and  $L_2$ , in the cases of HAR = 1.0 and 0.5, there is a local peak of  $I_U$  that exceeds  $I_0$  at about  $z/H = 1.03$ – $1.04$ . Above the local peak of  $I_U$  to  $z/H = 1.3$ , there is a height range of favorable or relatively favorable wind conditions ( $I_U/I_0 \leq 1$  and  $\bar{U}/U_0 \geq 1$  or at least  $\bar{U}/U_0 \geq 0.97$ ). At  $L_2$ , in the case of HAR = 0.25, the maximum value of the local peak of  $I_U$  is less than  $I_0$ , and the bottom of the height range of favorable or relatively favorable wind conditions is low being at about  $z/H = 1.01$ . On the other hand, at  $L_1$ , in the case of HAR = 0.25, the bottom of the height range is relatively high being at about  $z/H = 1.08$ . Therefore, in the case of HAR = 0.25, as compared to  $L_2$  (shorter windward edge's midpoint),  $L_1$  (longer windward edge's midpoint) is not appropriate for SWT installation at low heights.

At windward corner B in all HAR cases, the wind condition is not favorable as compared to those at other windward locations because  $\bar{U}$  is significantly smaller ( $\bar{U}/U_0 \approx 0.95$ ) although  $I_U$  is less than  $I_0$  at a height range of  $z/H \approx 1.0$  to 1.15.

At leeward locations  $L_3$ – $L_5$  and D, in all HAR cases, the bottoms of the height range of favorable wind conditions ( $I_U/I_0 \leq 1$  and  $\bar{U}/U_0 \geq 1$ ) are higher than those of the favorable or relatively favorable wind conditions at the windward locations. However, the favorable wind conditions at the leeward locations are generally better than those at the windward locations. With a decrease in HAR, the bottoms of the height range at the leeward locations generally decrease. However, there are some exceptions, such as the case of  $\alpha = 22.5^\circ$ . At corner D, the bottom of the height range is higher when HAR = 0.5 than when HAR = 1.0, and at  $L_5$  and  $L_3$ , the bottom of the height range is higher when HAR = 0.25 than when HAR = 0.5. In all HAR cases,  $L_5$  is the leeward location where the bottom of the favorable wind conditions is the lowest.

### 3.2.4. Wind Direction $\alpha = 67.5^\circ$

In all HAR cases, at windward corners A, B, and C, there is a height range where  $I_U/I_0 \leq 1$  from low heights ( $z/H \approx 1.02$ – $1.05$ ) to higher heights ( $z/H \approx 1.15$  or higher). At corner A, the wind conditions are favorable in the height range where  $I_U/I_0 \leq 1$ , especially at relatively low heights ( $z/H < 1.1$ ) being  $\bar{U}/U_0 \geq 1.05$ . At corner B, in the height range where  $I_U/I_0 \leq 1$ , the wind conditions are relatively favorable when HAR = 1.0 being  $\bar{U}/U_0 \approx 0.97$ . However, those are worse when HAR = 0.5 and 0.25 with  $\bar{U}/U_0 < 0.97$ . This tendency is caused by the stagnation point moving toward corner B with a decrease in HAR. From Figure 5(b,g,l), it is confirmed that the position with the most decreased wind speed region upwind of the building moves to corner B with a decrease in HAR. At corner C, the wind conditions are favorable or relatively favorable being  $\bar{U}/U_0 \approx 1$  in the height range where  $I_U/I_0 \leq 1$ . With a decrease in HAR,  $\bar{U}/U_0$  at C at low heights ( $z/H < 1.1$ ) recovers slightly due to the stagnation point moving to corner B.

At the windward edge's midpoint  $L_1$  in all HAR cases, the wind conditions are favorable from low heights ( $z/H \approx 1.01$ – $1.04$ ) to higher heights ( $z/H \approx 1.3$  or higher) like that at corner A. The values of  $\bar{U}$  at  $L_1$  at low heights ( $z/H \leq 1.1$ ) are slightly lower when HAR = 0.5 and 0.25, compared with those when HAR = 1.0, because of the stagnation point moving toward corner B.

At the windward edge's midpoint  $L_2$ , there is a height range where  $I_U/I_0 \leq 1$  from relatively low heights ( $z/H \approx 1.03$ – $1.06$ ) to higher heights ( $z/H \approx 1.2$  or higher). The bottom of the height range where  $I_U/I_0 \leq 1$  decreases with a decrease in HAR. In the height range where  $I_U/I_0 \leq 1$ , the wind conditions at low heights ( $z/H \leq 1.1$ ) are not favorable when HAR = 1.0 being  $\bar{U}/U_0 < 0.97$ . However, the bottom of the height range where  $\bar{U}/U_0 \geq 0.97$  decreases with a decrease in HAR. When HAR = 0.25, the bottom of the relatively favorable wind conditions is low being at about  $z/H = 1.04$ .

At leeward locations  $L_3$ – $L_5$  and D, in all HAR cases, the bottoms of the height range of favorable wind conditions ( $I_U/I_0 \leq 1$  and  $\bar{U}/U_0 \geq 1$ ) are higher than those of the favorable or relatively

favorable wind conditions at the windward locations. However, the favorable wind conditions at the leeward locations are generally better than those at the windward locations. With a decrease in HAR, the bottoms of the height range at all leeward locations decrease. The order of the bottoms of the height range at the leeward locations in the case of HAR = 1.0 is the same as that in the case of HAR = 0.25. However, it is different from that in the case of HAR = 0.5. When HAR = 1.0 and 0.25, the bottoms of the height range at L<sub>5</sub> are the lowest, but when HAR = 0.5, the bottoms of the height range at L<sub>4</sub> are slightly lower than that at L<sub>5</sub>. It is remarkable that the bottom of the height range at L<sub>5</sub>, in the case of HAR = 0.25, is very low ( $z/H \approx 1.04$ ).

### 3.2.5. Wind Direction $\alpha = 90^\circ$

At windward corners B and C, the bottoms of the height range of favorable or relatively favorable wind conditions ( $I_U/I_0 \leq 1$  and  $\bar{U}/U_0 \geq 1$  or at least  $\bar{U}/U_0 \geq 0.97$ ) increase from  $z/H \approx 1.04$  to  $z/H \approx 1.06$  with a decrease in HAR. In addition, the tops of the favorable or relatively favorable wind conditions decrease significantly with a decrease in HAR. In the height range of favorable or relatively favorable wind conditions,  $\bar{U}/U_0 \approx 1.0$ .

At the windward edge's midpoint L<sub>2</sub>, the wind conditions are not favorable at low heights ( $z/H < 1.1$ ) in the cases of HAR = 1.0 and 0.5. When HAR = 0.25, the wind conditions are relatively favorable ( $I_U/I_0 \approx 1.0$  and  $\bar{U}/U_0 \approx 1.0$ ) at  $z/H \approx 1.1$ .

At leeward locations L<sub>1</sub>, L<sub>3</sub>–L<sub>5</sub>, A and D, the bottoms of the height range, where  $I_U/I_0 \leq 1$ , are higher than those at the leeward corners except at A, D, and L<sub>4</sub> in the case of HAR = 0.25. In the case of HAR = 0.25, at A, D, and L<sub>4</sub>, there is no height range where  $I_U/I_0 \leq 1$ . At the leeward locations,  $\bar{U}/U_0$  in the height range where  $I_U/I_0 \leq 1$  decreases significantly with a decrease in HAR. When HAR = 1.0, the wind conditions in the same height range at all the leeward locations are more favorable than those at the windward corners. However, when HAR = 0.5, the wind conditions in the height range where  $I_U/I_0 \leq 1$  at L<sub>1</sub>, L<sub>3</sub>, and L<sub>5</sub> are more favorable than the wind conditions in the height range where  $I_U/I_0 \leq 1$  at the windward corners. The wind conditions in this height range at A, D, and L<sub>4</sub> are about as good as those at the windward corners. Moreover, when HAR = 0.25, the wind conditions in the height range where  $I_U/I_0 \leq 1$ , at L<sub>1</sub>, L<sub>3</sub>, and L<sub>5</sub>, are as good as those at the windward corners. Like  $\alpha = 0^\circ$ , the order of the bottoms of the height range of favorable wind conditions at the leeward locations does not change with a decrease in HAR. At L<sub>1</sub> and L<sub>3</sub>, which are the midpoints of the edges parallel to the wind direction, the bottoms of the height range are lowest among the leeward locations.

### 3.3. Wind Conditions at Representative Roof Locations with No Prevailing Wind Direction

Figures 11 and 12 show the vertical profiles of  $\bar{U}/U_0$  and  $I_U/I_0$ , respectively, at corner A, at long-edge's midpoint L<sub>1</sub> and short-edge's midpoint L<sub>4</sub> and the center L<sub>5</sub> of the roof under a condition with no prevailing wind direction. This condition assumes that the frequencies of the occurrence of 16 wind directions in increments of  $22.5^\circ$  are equal, and the profiles of  $\bar{U}$  and  $I_U$  of the approaching wind in each direction are the same as those in Figure 3. That is, the profiles in Figures 11 and 12 were obtained by averaging the profiles of  $\bar{U}/U_0$  and  $I_U/I_0$  over 16 wind directions by considering the symmetrical relationship between wind direction and the representative locations on the roof. For example, the wind profile at corner A, in the case of  $\alpha = 202.5^\circ$ , is considered to be the same as that at corner C, in the case of  $\alpha = 22.5^\circ$ . Table A2 in Appendix A summarizes the height ranges of relatively favorable wind conditions ( $\bar{U}/U_0 \geq 0.97$  and  $I_U/I_0 \leq 1$ ) at A, L<sub>1</sub>, L<sub>4</sub>, and L<sub>5</sub>.

The bottoms of the height ranges of the favorable wind conditions where  $I_U/I_0 \leq 1$  and  $\bar{U}/U_0 > 1$  decrease with a decrease in HAR. At L<sub>5</sub> when HAR = 1.0 or at L<sub>4</sub> when HAR  $\leq$  0.5, the bottom of the height range of favorable wind conditions is lowest; the bottoms of the height ranges at these locations are almost the same when HAR = 0.5 and 0.25.

In the height range of favorable wind conditions at each location in all HAR cases,  $\bar{U}/U_0$  at  $L_5$  is greater than or equal to  $\bar{U}/U_0$  at  $A$ ,  $L_1$ , and  $L_4$ . Therefore, in the condition with no prevailing wind direction, the center of the roof is the most optimal location for installing SWTs.

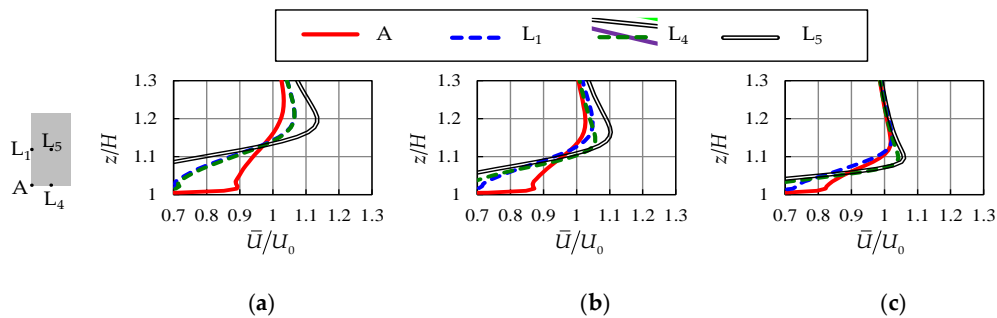


**Figure 11.** Vertical profiles of horizontal wind velocity ratios at representative locations on the roof, in the case of no prevailing wind direction. (a) HAR = 1.00; (b) HAR = 0.50; (c) HAR = 0.25.

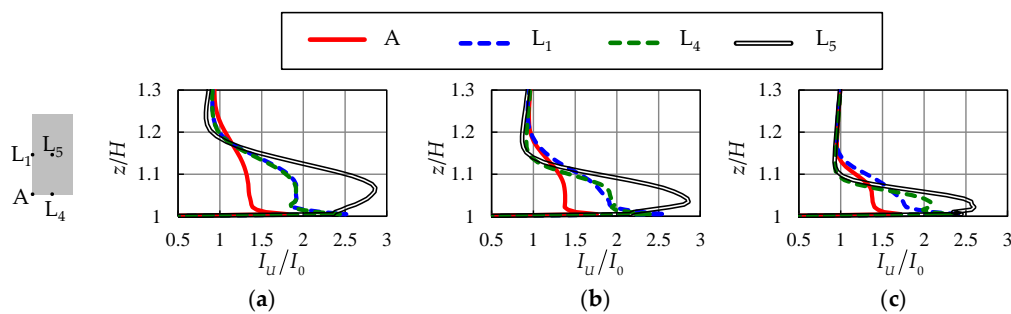


**Figure 12.** Vertical profiles of turbulence intensity ratios at representative locations on the roof, in the case of no prevailing wind direction. (a) HAR = 1.00; (b) HAR = 0.50; (c) HAR = 0.25.

In the height range of favorable wind conditions at  $L_4$ , the maximum value of  $\bar{U}/U_0$  at  $L_4$  is almost the same as that at  $L_1$  when HAR = 0.5 and is significantly larger than that at  $L_1$  when HAR = 0.25. Considering that the bottom of the height range is lowest at  $L_4$  when HAR = 0.5 and 0.25, this location is more favorable for installing SWTs than  $L_1$ .

At corner A, the bottom of the height range of favorable wind conditions is significantly higher than those at  $L_4$  and  $L_5$ . In addition, in the height range,  $\bar{U}/U_0$  at corner A is smaller than that at  $L_4$  and  $L_5$ . Therefore, for all HAR cases, in the height range at corner A, it is less favorable to install SWTs at corner A than at  $L_4$  and  $L_5$ . However, near the roof surface,  $I_U/I_0$  and  $\bar{U}/U_0$  are significantly smaller and larger, respectively, than they are at  $L_1$ ,  $L_4$ , and  $L_5$ . Therefore, when it is necessary to install SWTs near the roof surface, above  $z/H \approx 1.02$ , it is recommended to install those that are tolerant of  $I_U/I_0 \approx 1.45$  at corner A. It will then be possible to obtain more power output than at  $L_1$ ,  $L_4$ , and  $L_5$ . In cases where there is a prevailing wind direction, SWTs that are tolerant of  $I_U/I_0 \approx 1.45$  can also be installed at almost all of the windward corners above  $z/H \approx 1.02$ , except for corner C when  $\alpha = 22.5^\circ$  and HAR = 0.25. Considering the relatively large values of  $\bar{U}/U_0$ , the development of a new IEC design class for SWTs to be installed near the roof surface at windward corners with a prevailing wind direction or at corners with no prevailing wind direction can significantly increase the opportunities for installing SWTs near the roof surface.

#### 4. Conclusions

From the viewpoint of installing small wind turbines (SWTs) on rooftops, we investigated the effects of wind direction  $\alpha$  and the horizontal aspect ratio (HAR = width/length) of a high-rise cuboid building on wind conditions over the roof. This was done by performing large eddy simulations

of wind flow around a scale model building with an equivalent height and length of 80 and 40 m, respectively. The respective HARs were 1.0, 0.5, and 0.25. We defined  $\alpha$  as the angle between the vector of the stream-wise wind direction and the normal vector of the building's leeward face with longer roof edge. In addition, we defined the roof's center, corners, and the midpoints of each edge as representative locations. The main findings are summarized as follows:

- (1) The magnitude of the mean horizontal wind velocity  $\bar{U}$  over the roof significantly depends on the length of the windward edge of the roof. The variation in  $\bar{U}$  over the roof tends to become smaller with a decrease in HAR. This tendency is more prominent as  $\alpha$  increases.
- (2) At the windward corners of the roof, wind conditions are generally favorable at relatively low heights. However, when  $\text{HAR} \leq 0.5$  and  $\alpha = 22.5^\circ$ , the bottom of the height range of favorable wind conditions at the windward corner between the roof's shorter windward edge and its longer leeward edge is relatively high. In addition, when  $\alpha = 45^\circ$  or when  $\text{HAR} \leq 0.5$  and  $\alpha = 67.5^\circ$ ,  $\bar{U}$  at the windward corner between the two windward edges is low.
- (3) In many cases with HAR and  $\alpha$ , wind conditions at the midpoint of the roof's windward edge are not favorable at relatively low heights. When  $\alpha = 0^\circ$  or  $90^\circ$ , wind conditions at this location are not favorable at relatively low heights. In addition, when  $\alpha = 22.5^\circ$  or  $\text{HAR} = 0.25$  and  $45^\circ$ , the wind conditions at the midpoint of the roof's windward longer edge are not favorable at relatively low heights.
- (4) At the leeward locations of the roof, the bottoms of the height range of favorable wind conditions are generally higher than those at the windward locations, but the favorable wind conditions are much better than those at the windward locations. When  $\alpha = 0^\circ$  or  $90^\circ$ , the order of the bottoms of the height range of favorable wind conditions at the leeward roof locations does not change with HAR; the bottom of the height range at the midpoints of the roof's edges parallel to the wind direction is lowest among the leeward representative locations. In addition, when  $\alpha = 45^\circ$ , the bottom of the height range at the center of the roof is lowest among the leeward representative locations.
- (5) Under the condition where there is no prevailing wind direction, the center of the roof is the most optimal location for installing SWTs. In addition, compared with the midpoints of the roof's long edges, the midpoints of the roof's short edges are more favorable for installing SWTs. Moreover, it is less favorable to install SWTs at the corners of the roof than at the center and midpoints of the roof's short edges. However, although the turbulence intensity is significantly larger than that of undisturbed wind, at relatively low heights at the corners, the turbulence intensity and wind velocity are significantly smaller and larger, respectively, than those at other representative locations.

It is important to understand the applicability of the findings of this study. As a future study, it is necessary to investigate the effects of HAR by increasing one of the sides of the buildings, instead of decreasing it as in the present study. It is also necessary to investigate the effects of Reynolds number on the flow characteristics over the roof.

**Acknowledgments:** This research was supported by the project "Research and Development of Next-Generation Wind Power Generation Technology & Research and Development of Basic and Applied Technologies" of NEDO (New Energy and Industrial Technology Development Organization). The computation was mainly carried out using the computer facilities at Hokkaido University.

**Author Contributions:** Takaaki Kono performed the numerical simulations. Takaaki Kono analyzed the data with supervision by Tetsuya Kogaki and Takahiro Kiwata.

**Conflicts of Interest:** The authors declare no conflict of interest.

## Appendix A

Table A1 summarizes the height ranges of relatively favorable wind conditions ( $\bar{U}/U_0 \geq 0.97$  and  $I_U/I_0 \leq 1$ ) at the representative locations on the roof for all run cases with a prevailing wind

direction. In addition, Table A2 summarizes the height ranges of relatively favorable wind conditions ( $\bar{U}/U_0 \geq 0.97$  and  $I_U/I_0 \leq 1$ ) at representative locations on the roof in the case of no prevailing wind direction.

**Table A1.** Height ranges of relatively favorable wind conditions ( $\bar{U}/U_0 \geq 0.97$  and  $I_U/I_0 \leq 1$ ) at the representative locations on the roof for all run cases with a prevailing wind direction. The height ranges are normalized by the height of the buildings,  $H$ . The height above  $z/H = 1.50$  is not considered. “NHR” stands for “no height range of relatively favorable conditions”.

Run Case	Representative Location on the Roof								
	A	B	C	D	L <sub>1</sub>	L <sub>2</sub>	L <sub>3</sub>	L <sub>4</sub>	L <sub>5</sub>
100_000	1.05–1.33	1.05–1.33	1.25–1.50	1.26–1.50	1.20–1.26	1.18–1.48	1.29–1.50	1.19–1.50	1.22–1.48
100_225	1.05–1.43	1.03–1.23	1.03–1.48	1.26–1.50	1.14–1.36	1.05–1.43	1.19–1.50	1.20–1.50	1.19–1.5
100_450	1.03–1.50	NHR	1.02–1.46	1.16–1.50	1.03–1.38	1.06–1.38	1.19–1.50	1.19–1.50	1.11–1.48
050_000	1.04–1.29	1.04–1.32	1.19–1.48	1.19–1.50	1.20–1.26	1.13–1.42	1.23–1.48	1.13–1.42	1.16–1.42
050_225	1.06–1.43	1.04–1.23	1.07–1.43	1.23–1.50	1.18–1.28	1.07–1.36	1.21–1.48	1.15–1.48	1.15–1.41
050_450	1.03–1.47	NHR	1.02–1.36	1.18–1.48	1.05–1.33	1.04–1.31	1.12–1.43	1.15–1.46	1.10–1.39
050_675	1.03–1.39	NHR	1.04–1.31	1.16–1.39	1.06–1.34	1.09–1.25	1.16–1.39	1.18–1.39	1.13–1.38
050_900	1.18–1.29	1.08–1.20	1.06–1.22	1.18–1.29	1.13–1.34	1.13–1.20	1.13–1.33	1.19–1.29	1.15–1.34
025_000	1.04–1.25	1.05–1.31	1.14–1.41	1.14–1.45	NHR	1.09–1.38	1.16–1.43	1.09–1.38	1.12–1.36
025_225	1.02–1.38	1.04–1.16	1.09–1.36	1.15–1.46	NHR	1.06–1.31	1.16–1.41	1.11–1.43	1.12–1.34
025_450	1.02–1.41	NHR	1.02–1.29	1.15–1.43	1.07–1.30	1.01–1.23	1.13–1.38	1.11–1.41	1.10–1.34
025_675	1.03–1.28	NHR	1.03–1.21	1.11–1.29	1.02–1.26	1.04–1.19	1.11–1.29	1.09–1.29	1.06–1.29
025_900	NHR	1.07–1.12	1.07–1.12	NHR	1.10–1.20	NHR	1.10–1.19	NHR	1.12–1.20

**Table A2.** Height ranges of relatively favorable wind conditions ( $\bar{U}/U_0 \geq 0.97$  and  $I_U/I_0 \leq 1$ ) at the representative locations on the roof in the case of no prevailing wind direction. The height ranges are normalized by the height of the buildings,  $H$ .

HAR	Representative Location on the Roof			
	A	L <sub>1</sub>	L <sub>4</sub>	L <sub>5</sub>
1.00	1.23–1.48	1.20–1.48	1.20–1.49	1.18–1.49
0.50	1.18–1.38	1.18–1.40	1.13–1.38	1.13–1.41
0.25	1.13–1.31	1.14–1.31	1.09–1.30	1.10–1.31

## References

- Smith, J.; Forsyth, T.; Sinclair, K.; Oteri, F. *Built-Environment Wind Turbine Roadmap*; Technical Report NREL/TP-5000-50499; National Renewable Energy Laboratory: Golden, CO, USA, 2012.
- Manwell, J.F.; MCGowan, J.G.; Rogers, A.L. *Wind Energy Explained Theory, Design and Application*, 2nd ed.; Wiley: Chichester, UK, 2009; p. 33 and 63.
- Tieleman, H.W. Wind tunnel simulation of wind loading on low-rise structures: A review. *J. Wind Eng. Ind. Aerodyn.* **2003**, *91*, 1627–1649. [[CrossRef](#)]
- Ahmad, K.; Khare, M.; Chaudhry, K.K. Wind tunnel simulation studies on dispersion at urban street canyons and intersections—a review. *J. Wind Eng. Ind. Aerodyn.* **2005**, *93*, 697–717. [[CrossRef](#)]
- Blocken, B. 50 years of Computational Wind Engineering: Past, present and future. *J. Wind Eng. Ind. Aerodyn.* **2014**, *129*, 69–102. [[CrossRef](#)]
- Blackmore, P. *Building-Mounted Micro-Wind Turbines on High-Rise and Commercial Buildings*; IHS BRE Press: Watford, UK, 2010; pp. 1–18.
- Kono, T.; Kogaki, T. Numerical investigation of wind conditions over a rectangular prism-shaped building for mounting small wind turbines. *Wind Eng.* **2012**, *36*, 111–121. [[CrossRef](#)]
- Toja-Silva, F.; Peralta, C.; Lopez-Garcia, O.; Navarro, J.; Cruz, I. Roof region dependent wind potential assessment with different RANS turbulence models. *J. Wind Eng. Ind. Aerodyn.* **2015**, *142*, 258–271. [[CrossRef](#)]
- Mertens, S. The energy yield of roof mounted wind turbines. *Wind Eng.* **2003**, *27*, 507–518. [[CrossRef](#)]

10. Heath, M.A.; Walshe, J.D.; Watson, S.J. Estimating the potential yield of small building-mounted wind turbines. *Wind Energy* **2007**, *10*, 271–287. [[CrossRef](#)]
11. Blackmore, P. *Siting Micro-Wind Turbines on House Roofs*; IHS BRE Press: Watford, UK, 2008; pp. 1–25.
12. Guerri, O.; Sakout, A.; Hamdouni, A. Numerical simulation of the fluid flow around a roof mounted wind turbine. *Wind Eng.* **2010**, *34*, 501–516. [[CrossRef](#)]
13. Ledo, L.; Kosasih, P.B.; Cooper, P. Roof mounting site analysis for micro-wind turbines. *Renew. Energy* **2011**, *36*, 1379–1391. [[CrossRef](#)]
14. Abohela, I.; Hamza, N.; Dudek, S. Effect of roof shape, wind direction, building height and urban configuration on the energy yield and positioning of roof mounted wind turbines. *Renew. Energy* **2013**, *50*, 1106–1118. [[CrossRef](#)]
15. Tabrizi, T.B.; Whale, J.; Lyons, T.; Urmee, T. Performance and safety of rooftop wind turbines: Use of CFD to gain insight into inflow conditions. *Renew. Energy* **2014**, *67*, 242–251. [[CrossRef](#)]
16. International Electrotechnical Commission (IEC). *Wind Turbines-Part 2: Design Requirements for Small Wind Turbines*; International Electrotechnical Commission (IEC): Geneva, Switzerland, 2013; pp. 29–39.
17. Pierik, J.T.G.; Dekker, J.W.M.; Braam, H.; Bulder, B.H.; Winkelaar, D.; Larsen, G.C.; Morfiadakis, E.; Chaviaropoulos, P.; Derrick, A.; Molly, J.P. Wind energy for the next millennium. In Proceedings of the European Wind Energy Conference, Nice, France, 1–5 March 1999.
18. Tamura, Y.; Ohkuma, T.; Okada, H.; Kanda, J. Wind loading standards and design criteria in Japan. *J. Wind Eng. Ind. Aerodyn.* **1999**, *83*, 555–566. [[CrossRef](#)]
19. Mohamed, M.A.; Wood, D.H. Modifications to Reynolds-averaged Navier-Stokes turbulence models for the wind flow over buildings. *Int. J. Sustain. Energy* **2015**, 1–17. [[CrossRef](#)]
20. Meng, Y.; Hibi, K. Turbulent measurements of the flow field around a high-rise building. *J. Wind Eng.* **1998**, *76*, 55–64. (In Japanese) [[CrossRef](#)]
21. Smagorinsky, J. General circulation experiments with the primitive equations. *Mon. Weather Rev.* **1991**, *91*, 99–164. [[CrossRef](#)]
22. Van-Driest, E.R. On turbulent flow near a wall. *J. Aeronaut. Sci.* **1956**, *23*, 1007–1011. [[CrossRef](#)]
23. Germano, M.; Piomelli, U.; Moin, P.; Cabot, W.H. A dynamic subgrid scale eddy viscosity model. *Phys. Fluids A* **1991**, *3*, 1760–1765. [[CrossRef](#)]
24. Lilly, D.K. A proposed modification of the Germano subgrid-scale closure method. *Phys. Fluids A* **1992**, *4*, 633–635. [[CrossRef](#)]
25. Rodi, W. Comparison of LES and RANS calculations of the flow around bluff bodies. *J. Wind Eng. Ind. Aerodyn.* **1997**, *69–71*, 55–75. [[CrossRef](#)]
26. Murakami, S.; Iisuka, S.; Ooka, R. CFD analysis of turbulent flow past square cylinder using dynamic LES. *J. Fluids Struct.* **1999**, *13*, 1097–1112. [[CrossRef](#)]
27. Sohankar, A.; Davidson, L.; Norberg, C. Large eddy simulation of flow past a square cylinder: Comparison of different subgrid scale models. *J. Fluids Eng.* **1999**, *122*, 39–47. [[CrossRef](#)]
28. Ferziger, J.H.; Peric, M. *Computational Methods for Fluid Dynamics*, 3rd ed.; Springer: Berlin/Heidelberg, Germany, 2002; pp. 281–283.
29. Kataoka, H.; Mizuno, M. Numerical flow computation around 3D square cylinder using inflow turbulence. *J. Archit. Plan. Environ. Eng. (Trans. AIJ)* **1999**, *523*, 71–77. (In Japanese) [[CrossRef](#)]
30. Kataoka, H. Numerical simulations of a wind-induced vibrating square cylinder within turbulent boundary layer. *J. Wind Eng. Ind. Aerodyn.* **2008**, *96*, 1985–1997. [[CrossRef](#)]
31. Zephyr9000. Available online: <https://www.zephyreco.co.jp/en/products/z-9000.jsp> (accessed on 17 October 2016).
32. Irwin, P.; Denoon, R.; Scott, D. *Wind Tunnel Testing of High-Rise Buildings*; Taylor & Francis: Abingdon, UK, 2013; p. 19.
33. Toja-Silva, F.; Peralta, C.; Lopez-Garcia, O.; Navarro, J.; Cruz, I. Effect of roof-mounted solar panels on the wind energy exploitation on high-rise buildings. *J. Wind Eng. Ind. Aerodyn.* **2015**, *145*, 123–138. [[CrossRef](#)]

